short communications

The pilus-retraction protein PilT: ultrastructure of the biological assembly

Katrina T. Forest,*‡ Kenneth A. Satyshur, Gregory A. Worzalla, Johanna K. Hansen and Timothy J. Herdendorf§

Department of Bacteriology, University of Wisconsin-Madison, USA

‡ Address for correspondence: 420 Henry Mall, Madison, WI 53706, USA.
§ Current address: Medical College of Wisconsin, Milwaukee, WI 53226, USA.

Correspondence e-mail: forest@bact.wisc.edu

PilT is a biological motor required for the retraction of bacterial type IV pili. *Nesseria gonorrhoeae* PilT has been purified and its ultrastructure has been examined by freeze-etch electron microscopy, revealing a 115 Å outer diameter, 15−35 Å inner diameter ring. *Aquifex aeolicus* PilT crystals were obtained in a primitive hexagonal space group (unit-cell parameters $a = b = 107.3$, $c = 68.5$ Å) and diffract to a minimum Bragg spacing of 2.8 Å when PilT is co-crystallized with adenine nucleotides. Initial phases to 3.5 Å resolution have been determined by multiwavelength anomalous dispersion and density modification. Resulting electron-density maps show a hexameric *A. aeolicus* PilT ring 105 Å wide by 55 Å high, with an inner cavity that varies in shape and width from 20 to 40 Å over the height of the complex. Both PilT ultrastructures are very similar to type II and type IV secretion ATPases in overall shape, size and assembly.

1. Introduction

PilT proteins are required for the retraction of type IV pilus filaments in Gram-negative bacteria. This retraction drives surface motility in a fishing-reel fashion: a bacterium adhered to a solid substrate *via* an extracellular hair-like type IV pilus is pulled forward as the pilus is reeled into the bacterium from its base (Bradley, 1972; Merz *et al.*, 2000; Skerker & Berg, 2001). The force generated by the pilus-retraction machinery is greater than 100 pN, making the retraction motor the strongest biological motor known (Maier *et al.*, 2002). PilT-mediated pilus retraction is required for phage-particle uptake (Bradley, 1980), DNA uptake for natural transformation (Wolfgang *et al.*, 1998; Meier *et al.*, 2002) and eukaryotic cell signalling in host–pathogen interactions (Merz *et al.*, 1999; Pujol *et al.*, 1999). PilT function is required for full virulence in animal as well as plant pathogens (Comolli *et al.*, 1999; Kang *et al.*, 2002). Furthermore, PilT is found in the genomes of more than 100 microbes from environmental niches as diverse as deep-sea thermal vents, bioremediation sites, animal gastrointestinal tracts and fresh water, implicating pilus retraction as a fundamental and evolutionarily conserved bacterial process.

Despite the important role of pilus retraction in microbial physiology, the molecular mechanism of retraction is not understood. Structures of type IVa pilin monomers, the presumed substrates of PilT, have been solved (Forest, 2004), but to date no PilT structures are known. *In vivo*, PilT can be found both associated with the inner membrane and in the cytoplasm (Brossay *et al.*, 1994; Okamoto & Ohmori, 2002). Purified PilT is an oligomeric NTPase (Herdendorf *et al.*, 2002; Okamoto & Ohmori, 2002) and disruption of the invariant lysine in the phosphate-binding loop abolishes ATPase activity *in vitro* (Herdendorf *et al.*, 2002) and pilus retraction *in vivo* (K. Aukema, submitted).

The core ATPase domain of PilT shares 30–50% homology with members of a large family of type II secretion ATPases involved in secretion of folded proteins across the outer membrane, assembly of type IV pili, retraction of type IV pili and natural competence in Gram-positive bacteria (Planet *et al.*, 2001). The only type II secretion ATPase whose structure is known is *Vibrio cholerae* EpsE, one of 14 extracellular secretion proteins required for secretion of cholera toxin (Robien *et al.*, 2003). Although PilT from *Nesseria gonorrhoeae* shares 36% sequence identity with EpsE in the 166 amino acids that make up the ATPase core, there is little recognizable sequence homology in the N-terminal and C-terminal domains. While their ATPase core structures may be expected to be similar, it remains an open question whether the low level of homology between PilT and EpsE in the two-thirds of the protein outside this region indicates a lack of structural homology or whether a similar structure may be maintained.

In order to illuminate the mechanism of pilus retraction and to understand the structural and functional differences between the distant members of the secretion ATPase family, we are carrying out a structural biology effort on several PilT proteins. Here, we report

the purification and electron-microscopy analysis of *N. gonorrhoeae* PilT and the crystallization, data collection and multi-wavelength anomalous dispersion phasing to 3.5 Å resolution of *Aquifex aeolicus* PilT.

2. Materials and methods

2.1. *N. gonorrhoeae* PilT overexpression and purification.

The *N. gonorrhoeae pilT* gene was cloned from strain MS11 genomic DNA by the polymerase chain reaction (PCR), utilizing a forward primer which incorporates the native start codon into an *Nde*I restriction site (5′-CTAAACAGAGCCGCC**CATAT-G**CAGATTACCGAC-3′; *Nde*I site in bold) and a reverse primer which anneals downstream of the natural stop codon (5′-TTGTTTT**GCGGCCGC**CATGGCCGGA-GCGGTT-3′; *Not*I site in bold). Using standard molecular-biology protocols, the PCR product was digested with *Nde*I and *Not*I, ligated into the multicloning site of pET23a+ (Novagen) which had been similarly digested and transformed into the *Escherichia coli* host strain JM109. The successful cloning to yield pET23a(+)-GCPilT was verified by automated DNA sequencing.

For purification, a 2 ml Luria Broth/ampicillin (100 µg ml^{-1}) (LB-amp) culture was inoculated with *E. coli* BL21(DE3)-pLysS harboring pET23a(+)GCPilT. This culture was incubated with shaking at 310 K until it reached mild turbidity, after which 100 µl was spread onto each of 12 LB-amp plates. After overnight incubation at 310 K, cells were scraped from these plates and inoculated into 2 l LB-amp with 2% ethanol. The large initial inoculum from the plates and the induction of stress-response proteins in response to ethanol were both intended to increase the overall yield of the potentially poorly soluble PilT. After 1 h incubated shaking at 294 K, cultures were induced with a final concentration of 1.0 m*M* isopropyl-*β*-D-thiogalactopyranoside (IPTG). 21 h post-induction, cells were harvested and cell pellets were resuspended in 50 ml lysis buffer [50 m*M* HEPES pH 7.8, 100 m*M* KCl, 20% glycerol, 1 U benzonase per millilitre (Novagen)]. After lysis by French press disintegration (four passes at 110 MPa), the total lysate was clarified by ultracentrifugation (100 000*g*, 90 min) and passed over a 2.5 × 18 cm Q-Sepharose anion-exchange column (Pharmacia) which had been pre-equilibrated in wash buffer (lysis buffer without benzonase). Pooled flowthrough fractions containing PilT were brought to

20 m*M* MgCl$_2$ and loaded in batch over 1 h at 277 K with gentle stirring onto 1.5 ml ATP-agarose (Sigma) or ATP*γ*S-agarose (see below) pre-equilibrated in wash buffer. A 1.0 × 2.0 cm column was packed with this resin and washed until the A_{280} fell below 0.005. Pure PilT was eluted with elution buffer (wash buffer with 20 m*M* MgCl$_2$ and 10 m*M* ATP pH 6.5) at a flow rate of 0.03 ml min^{-1}. The yield of PilT is approximately 1.5 mg from 2 l of culture.

Preparation of ATP*γ*S-agarose for use in purification of PilT was accomplished by oxidation of the nucleotide followed by coupling to activated agarose. For nucleotide oxidation, 9.5 m*M* sodium periodate was added slowly to cold neutral 10 m*M* ATP*γ*S solution. The reaction was allowed to proceed for 1 h at 273 K. For coupling to activated agarose, 4–5 µmol periodate-oxidized nucleotide in 0.1 *M* sodium acetate pH 5.0 was added to 1 ml adipic acid di-hydrazide agarose (Pierce) in the same buffer. The reaction was allowed to proceed for 3 h at 277 K, after which conjugated resin was washed with 1 *M* KCl. The extent of conjugation was determined by calculating the amount of free nucleotide remaining in the supernatant and wash fractions based on A_{260}.

2.2. *A. aeolicus* PilT expression and purification

The thermostable *A. aeolicus* PilT, with a C-terminal hexa-histidine purification tag, was overexpressed largely as described by Herdendorf *et al.* (2002). For seleno-L-methionine (SeMet) labeled protein, pET23a(+)-AaPilTC-His was transformed into B834(DE3)pLysS (Novagen), a methionine auxotroph (Leahy *et al.*, 1992), and cells were grown on LB agar plates containing both ampicillin (100 µg ml^{-1}) and chlor-amphenicol (34 µg ml^{-1}) (LB-amp/chlor). Overnight transformants were used to inoculate 100 ml LB-amp/chlor which was incubated at 310 K with shaking. After 16 h, 25 ml of this culture was inoculated into 1 l modified M9 minimal media plus anti-biotics and a nutrient mix containing amino acids and key vitamins (SelenoMet Nutrient Mix, Molecular Dimensions Inc.; Ramakrishnan *et al.*, 1993). The culture was allowed to grow for 1 h at 310 K before 4 ml of 10 mg ml^{-1} selenomethionine (Molecular Dimensions Inc.) was

added. Growth was allowed to continue for 4 h at 310 K before the temperature was lowered to 293 K and IPTG was added to a final concentration of 1 m*M* for expression. Expression was carried out for 20 h at 293 K and cells were harvested by centrifugation.

Purification of unlabeled and SeMet-labeled PilT were performed by Ni^{2+}-agarose affinity chromatography as described in Herdendorf *et al.* (2002). The overall yield of purified protein is typically 22 mg for native PilT and 4 mg for SeMet-labeled PilT expressed in 1 l of minimal media. Confirmation of complete SeMet labeling was determined through electro-spray ionization mass spectroscopy. Purified PilT was concentrated to 10–12 mg ml^{-1} for crystallization. In some instances, PilT purity was increased prior to crystallization by a 343 K heat-shock for 15 min followed by 30 min centriguation at 14 000*g* to remove any precipitated protein. SeMet-labeled protein retains the thermostability of the native *A. aeolicus* PilT.

2.3. Electron microscopy

Freeze-etch electron microscopy was carried out on purified *N. gonorrhoeae* PilT diluted to a final concentration of 16 µg ml^{-1} in cold KHMgE buffer (70 m*M* KCl, 30 m*M* HEPES pH 7.4, 1 m*M* MgCl$_2$, 3 m*M* EGTA) with 1 m*M* ATP as described previously (Heuser, 1993; Sexton *et al.*, 2004). Platinum replicas of frozen samples were photo-graphed at 68 000×, in stereo, on a Jeol transmission electron microscope.

2.4. Crystallization conditions

Crystallization conditions were first identified by use of sparse-matrix screening kits (Hampton Research). Optimization of initial conditions by varying both the
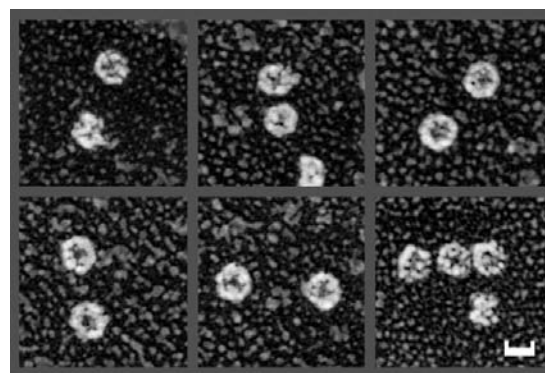

Figure 1
N. gonorrhoeae PilT forms rings of ∼115 Å in diameter. PilT was visualized by freeze-etch electron microscopy in the presence of ATP. PilT oligomers are mostly seen *en face*, although some side-on views are apparent (bottom oligomer in first, second and sixth frames). The scale bar represents 100 Å.
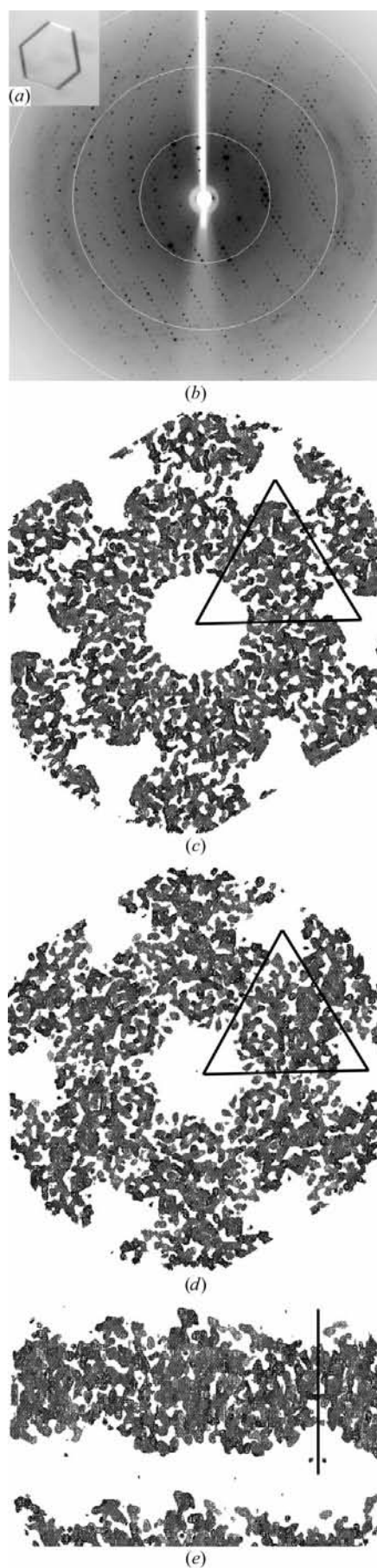
(a)

(b)

(c)

(d)

(e)

Figure 2
A. aeolicus PilT crystals yield high-quality data and experimental phases. (*a*) Hexagonal PilT–ATPγS crystal, dimensions ~0.1 × 0.1 × 0.02 mm. (*b*) Diffraction pattern from a similar PilT–ATPγS crystal showing resolution rings at 9.4, 4.7 and 3.1 Å. (*c*) Section from an *A. aeolicus* PilT electron-density map. To illustrate molecular boundaries, we have chosen to present a map calculated in *P*6 with solvent-flattened phases (using 50% solvent) at 3.5 Å resolution and contoured at 1.5σ. This 15 Å slice through the PilT ring is viewed down the crystallographic and molecular sixfold axis, with subunit boundaries indicated by a 62 Å edge equilateral triangle. (*d*) The subsequent 15 Å section. (*e*) A slab in the direction perpendicular to the previous views (on the same scale, with 62 Å ruler repeated) shows the tight lateral packing of hexamers and their height. The necessary interactions along the sixfold *z* axis that promote ordered crystal formation are potentially mediated by a poorly ordered loop or N- or C-terminal extension not visible in solvent-flattened electron-density maps.

Table 1
X-ray data-collection statistics.

Values in parentheses are the statistics for the indicated highest resolution shell. Statistics for all data sets are reported with Friedel pairs merged.

Data set	Se peak, ATP	Se remote, ATP	Native, ATP	Native, ATPγS
Wavelength (Å)	0.9794	0.9568	1.54	0.9792
Resolution (Å)	20–3.2 (3.37–3.2)	20–3.4 (3.58–3.4)	20–3.5 (3.79–3.6)	20–2.8 (2.95–2.8)
N_{meas}	79282 (11559)	64062 (9425)	74328 (9374)	59487 (8939)
N_{unique}	7481 (1093)	6295 (932)	5185 (746)	10698 (1600)
Completeness (%)	99.5 (100)	99.0 (97.1)	99.3 (99.3)	96.8 (98.4)
R_{merge} (%)	7.9 (25.6)	8.1 (20.1)	8.4 (20.2)	8.3 (19.5)
$\langle I/\sigma(I)\rangle$	7.9 (2.9)	5.5 (3.2)	6.6 (3.6)	6.0 (3.4)

concentration and pH of well components and also the initial conditions within the protein droplet led to an improved method in which a 4 µl drop containing 5–8 mg ml^{-1} protein in 5% glycerol, 75 m*M* KCl, 15% MPD, 180–250 m*M* NH$_4$SO$_4$, 100–170 m*M* imidazole, 15 m*M* Tris pH 7.9, 5–10 m*M* MgCl$_2$ and 1–5 m*M* ATP or 1 m*M* ATPγS is equilibrated at 293 K over an unbuffered 1 ml reservoir of 30–45% MPD, 0.2–0.4 *M* NH$_4$SO$_4$. Hexagonal plates appeared in 1–2 weeks.

2.5. Data collection, processing and MAD phasing

For data collection, crystals were cryopreserved directly from the mother liquor by plunging into liquid N$_2$. Native PilT–ATP and PilT–ATPγS diffraction data were measured on a Bruker Proteum CCD detector in-house or on a MAR CCD at Advanced Photon Source (APS) beamline 32-ID, respectively. MAD data were collected on a MAR CCD at APS beamline 14-ID-B. In-house data were processed with *SAINT* (Bruker Nonius). APS data were integrated, scaled and merged using the *CCP*4 programs *MOSFLM*, *SCALA* and *TRUNCATE*, respectively (Collaborative Computational Project, 1994) (Table 1).

Anomalous scattering centers were identified using *SHELX* (Schneider & Sheldrick, 2002) or *SOLVE* (Terwilliger & Berendzen, 1999) and refined using the *CCP*4 implementation of *MLPHARE*. Initial phases calculated from the refined selenium constellation were used to calculate electron-density maps which were subjected to solvent flattening using *DM* (Cowtan, 1994) over a range of estimated solvent contents.

3. Results and discussion

We have overexpressed and purified *N. gonorrhoeae* PilT to near-homogeneity. Gonococcal PilT has been difficult to work with and does not remain soluble above 1 mg ml^{-1} in aqeuous buffer for longer than several hours at 275 or 293 K after purification. Small irregular crystals have been obtained in crystallization trials set up immediately after purification, but thus far have not been suitable for data collection (data not shown). In order to assess the overall structure of the expected 228 kDa PilT oligomer, we instead turned to freeze-etch electron microscopy (Fig. 1). The micrographs reveal PilT rings of approximately 115 Å diameter with electron-poor central openings of approximately 15–35 Å diameter. Fine structure within the lumen can be discerned, while the perimeter of the rings is quite smooth (Fig. 1). Occasional PilT assemblies are seen tipped or side-on and these reveal the height of the rings to be at most 70 Å.

PilT from a second eubacterial species, the deep-sea thermal vent inhabitant *A. aeolicus*, has been shown to be thermostable and straightforward to overexpress and purify (Herdendorf *et al.*, 2002) and thus we have focused on this protein for crystallographic studies. Screening identified initial conditions which produced thin hexagonal plates. These grew with the same external morphology in the presence or absence of nucleotide, but the minimum Bragg spacing was substantially improved from ~15 Å for apo crystals to 7.5 Å for ATP co-crystals. Optimization lead to

reproducible PilT co-crystals with ATP or the non-hydrolyzable analogue ATPγS on equilibrating drops over a well of 0.2–0.4 M NH_4SO_4 and 30–45% MPD at neutral pH (Fig. 2a). These primitive hexagonal crystals, with unit-cell parameters $a = 107.3$, $b = 107.3$, $c = 68.5$ Å and a solvent content of 54.7%, contained a single 42.3 kDa monomer per asymmetric unit and diffracted to a maximum resolution of 2.8 Å (Table 1, Fig. 2b).

The improvement in diffraction quality of early PilT crystals when grown in the presence of ATP or ATPγS suggests that there is a reduction in mobility or structural heterogeneity upon nucleotide binding. (The enzymatic activity of *A. aeolicus* PilT is not detectable at 293 K and thus it is nucleotide binding rather than hydrolysis that leads to the improved order, even though ATP is likely to have undergone non-enzymatic hydrolysis to ADP during the weeks of room-temperature crystallization.) This clamping down may be similar to that observed for the type IV secretion ATPase HP0525 from *Helicobacter pylori*. In the presence of nucleotide, HP0525 attains a more compact structure as measured by velocity sedimentation and it crystallizes in a higher symmetry space group than in the absence of nucleotide (Savvides *et al.*, 2003). Our results are a preliminary indication of a similar phenomenon for PilT.

Selenomethionine-labeled PilT crystallizes under essentially identical conditions to native PilT. Based on the experimental fluorescence absorption spectrum, peak and high remote wavelengths were chosen and a two-wavelength MAD data set was collected from a single crystal to 3.2 and 3.4 Å resolution. Radiation damage limited our ability to collect data at a third wavelength. In $P6$ six major anomalous scattering centers were identified and refined similarly in *SHELX* or *SOLVE* (Terwilliger & Berendzen, 1999; Schneider & Sheldrick, 2002), corresponding to a subset of the ten methionines in this 42.7 kDa protein. The measurable anomalous signal for the peak data set only extends to ∼4.8 Å resolution, where the figure of merit for initial MAD phases correspondingly falls to ∼0.28. Phases calculated from refined selenium constellations including the six strongest sites were used to calculate electron-density maps, which were subjected to density modification and phase extension in *DM* over a wide range of estimated solvent contents. Solvent contents of 40–50% yielded the highest combined figures of merit (0.75–0.8 overall for 20–3.5 Å resolution, 0.5–0.7 for 3.6–3.5 Å), lowest real-space R_{free} values (13.5–

15%) and most interpretable electron-density maps (Figs. 2c, 2d and 2e). Although there were no systematic absences, phasing statistics were similar in space groups with a screw axis along the sixfold, and thus it is formally possible the PilT monomers are packed in a helical array.

The overall shape of the crystalline *A. aeolicus* PilT assembly appears to be a hexameric ring, in agreement with published gel-filtration measurements (Herdendorf *et al.*, 2002). The ultrastructure of the thermophilic PilT is the same as that of the mesophilic *N. gonorrhoeae* PilT protein analyzed by electron microscopy. Moreover, the overall size and shape of both PilTs is very similar to the type II secretion ATPase EpsE and the type IV secretion ATPase HP0525 (Robien *et al.*, 2003; Savvides *et al.*, 2003). The overall dimensions of the *A. aeolicus* PilT ring are 105 × 55 Å. The central cavity changes in shape from smooth-walled to star-shaped along the height of the complex, with an inner diameter ranging from ∼20 to 40 Å (Figs. 2c and 2d). The topologies of both faces of the PilT hexamer are gently curving, giving the appearance of protruding structural elements (Fig. 2e).

Two features of the calculated electron-density maps vary depending on the number of selenium sites used for initial phase determination, the resolution at which data are truncated for heavy-atom site refinement and the solvent content used for density modification, even though numerical statistics indicate similarly high-quality phases in each case. Firstly, some maps reveal a crown-shaped plug constricting the lumen of PilT. The biological relevance of this density, if any, is not yet clear. Secondly, no packing interactions of the top and bottom faces of PilT hexamers against one another were observed in density-modified electron-density maps until the solvent level was lowered to ∼40% (compared with the actual 54.7% level), indicating that the true contacts are likely to be sparse and explaining the preferred crystal growth in the plane of the PilT rings. These and other caveats of our moderate-resolution interpretation will be addressed upon phase extension, model building and structure refinement of PilT based on 2.8 Å resolution data which have recently been collected on ATPγS-containing PilT crystals (Table 1).

We have examined the low-resolution structure of the pilus-retraction protein PilT from two Gram-negative bacteria and demonstrated a shared ∼110 Å diameter hexameric ring architecture for PilT with other distantly related members of the large

type II/type IV secretion ATPase family. Further insights into the molecular mechanism of action of this remarkable nanomachinery await higher resolution crystallographic results and may also require *in vitro* conditions that more closely mimic the *in vivo* situation, for example co-crystallization with membrane lipids, pilin or components of the retraction machinery or pilus base.

References

Bradley, D. E. (1972). *J. Gen. Microbiol.* **72**, 303–319.

Bradley, D. E. (1980). *Can. J. Microbiol.* **26**, 146–154.

Brossay, L., Paradis, G., Fox, R., Koomey, M. & Hebert, J. (1994). *Infect. Immun.* **62**, 2302–2308.

Collaborative Computational Project, Number 4 (1994). *Acta Cryst.* D**50**, 760–763.

Comolli, J. C., Hauser, A. R., Waite, L., Whitchurch, C., Mattick, J. S. & Engel, J. N. (1999). *Infect. Immun.* **67**, 3625–3630.

Cowtan, K. (1994). *Jnt CCP4/ESF–EACBM Newsl. Protein Crystallogr.* **31**, 34–38.

Forest, K. T. (2004). *Structural Basis of Bacterial Pathogenesis*, edited by G. Waksman, S. J. Hultgren & M. G. Caparon. Washington, DC: ASM. In the press.

Herdendorf, T. J., McCaslin, D. & Forest, K. T. (2002). *J. Bacteriol.* **184**, 6465–6471.

Heuser, J. (1993). *J. Electron Microsc. Tech.* **13**, 244–263.

Kang, Y., Liu, H., Genin, S., Schell, M. A. & Denny, T. P. (2002). *Mol. Microbiol.* **46**, 427–437.

Leahy, D. J., Hendrickson, W. A., Aukhil, I. & Erickson, H. P. (1992). *Science*, **258**, 987–991.

Maier, B., Potter, L., So, M., Seifert, H. S. & Sheetz, M. P. (2002). *Proc. Natl Acad. Sci. USA*, **99**, 6012–16017.

Meier, P., Berndt, C., Weger, N. & Wackernagel, W. (2002). *FEMS Microbiol. Lett.* **207**, 75–80.

Merz, A. J., Enns, C. A. & So, M. (1999). *Mol. Microbiol.* **32**, 1316–1332.

Merz, A. J., So, M. & Sheetz, M. P. (2000). *Nature (London)*, **407**, 98–102.

Okamoto, S. & Ohmori, M. (2002). *Plant Cell Physiol.* **43**, 1127–1136.

Planet, P. J., Kachlany, S. C., DeSalle, R. & Figurski, D. H. (2001). *Proc. Natl Acad. Sci. USA*, **98**, 2503–2508.

Pujol, C., Eugene, E., Marceau, M. & Nassif, X. (1999). *Proc. Natl Acad. Sci. USA*, **96**, 4017–4022.

Ramakrishnan, V., Finch, J. T., Graziano, V., Lee, P. L. & Sweet, R. M. (1993). *Nature (London)*, **362**, 219–223.

Robien, M. A., Krumm, B. E., Sandkvist, M. & Hol, W. G. J. (2003). *J. Mol. Biol.* **333**, 657–674.

Savvides, S. N., Yeo, H. J., Beck, M. R., Blaesing,

F., Lurz, R., Lanka, E., Buhrdorf, R., Fischer, W., Haas, R. & Waksman, G. (2003). *EMBO J.* **22**, 1969–1980.

Schneider, T. R. & Sheldrick, G. M. (2002). *Acta Cryst.* D**58**, 1772–1779.

Sexton, J. A., Pinker, J. S., Roth, R., Heuser, J. E., Hultgren, S. J. & Vogel, J. P. (2004). *J. Bacteriol.* **186**, 1658–1666.

Skerker, J. M. & Berg, H. C. (2001). *Proc. Natl Acad. Sci. USA*, **98**, 6901–6904.

Terwilliger, T. C. & Berendzen, J. (1999). *Acta Cryst.* D**55**, 849–861.

Wolfgang, M., Lauer, P., Park, H. S., Brossay, L., Hebert, J. & Koomey, M. (1998). *Mol. Microbiol.* **29**, 321–330.